EphB1 interaction with caveolin-1 in endothelial cells modulates caveolae biogenesis

Chinnaswamy Tiruppathi[a,b,*], Sushil C. Regmi[a], Dong-Mei Wang[a], Gary C. H. Mo[a], Peter T. Toth[a], Stephen M. Vogel[a], Radu V. Stan[c], Mark Henkemeyer[d], Richard D. Minshall[a,b,e], Jalees Rehman[a], and Asrar B. Malik[a,b,*]

[a]Departments of Pharmacology and [e]Anesthesiology, and [b]The Center for Lung and Vascular Biology, The University of Illinois College of Medicine, Chicago, IL 60612; [c]Department of Pathology, Geisel School of Medicine, Dartmouth College, Hanover, NH 03755; [d]Departments of Neuroscience and Developmental Biology, University of Texas Southwestern Medical Center, Dallas, TX 75390

ABSTRACT **Caveolae, the cave-like structures abundant in endothelial cells (ECs), are important for multiple signaling processes such as production of nitric oxide and caveolae-mediated intracellular trafficking. Using superresolution microscopy, fluorescence resonance energy transfer, and biochemical analysis, we observed that the EphB1 receptor tyrosine kinase constitutively interacts with caveolin-1 (Cav-1), the key structural protein of caveolae. Activation of EphB1 with its ligand Ephrin B1 induced EphB1 phosphorylation and the uncoupling EphB1 from Cav-1 and thereby promoted phosphorylation of Cav-1 by *Src*. Deletion of Cav-1 scaffold domain binding (CSD) motif in EphB1 prevented EphB1 binding to Cav-1 as well as *Src*-dependent Cav-1 phosphorylation, indicating the importance of CSD in the interaction. We also observed that Cav-1 protein expression and caveolae numbers were markedly reduced in ECs from EphB1-deficient (*EphB1*$^{-/-}$) mice. The loss of EphB1 binding to Cav-1 promoted Cav-1 ubiquitination and degradation, and hence the loss of Cav-1 was responsible for reducing the caveolae numbers. These studies identify the crucial role of EphB1/Cav-1 interaction in the biogenesis of caveolae and in coordinating the signaling function of Cav-1 in ECs.**

Monitoring Editor
Asma Nusrat*
University of Michigan

Received: Dec 20, 2019
Revised: Feb 24, 2020
Accepted: Mar 25, 2020

INTRODUCTION

Caveolae, the plasma membrane invaginations on the luminal side of endothelial cell monolayer and the caveolae associated protein caveolin-1 (Cav-1), have a key homeostatic role in regulating caveolar functions such as the production of nitric oxide and caveolae-mediated trafficking (Predescu *et al.*, 2004, 2007; Frank *et al.*, 2009). Cav-1 is inserted into the caveolar plasma membrane where it serves as a primary structural and signaling protein (Palade, 1953; Predescu and Palade, 1993; Parton and del Pozo, 2013; Cheng and Nichols, 2016; Busija *et al.*, 2017). Mice with genetic deletion of Cav-1 (*Cav-1*$^{-/-}$) failed to form caveolae (Drab *et al.*, 2001; Schubert *et al.*, 2002) indicating the requirement of Cav-1 in caveolae biogenesis. Studies also showed that *Src* kinase-mediated phosphorylation of Cav-1 on Y-14 was required for the fission of caveolae from the plasma membrane and caveolae-mediated endocytosis and trafficking (Minshall *et al.*, 2000; Shajahan *et al.*, 2004; Zimnicka *et al.*, 2016). The Cav-1 scaffold domain (CSD) binds various signaling proteins via the sequence in CSD-interacting proteins, the CSD binding motif (CSDBM). These proteins include *Src* tyrosine kinases, eNOS (endothelial nitric oxide synthase), and trimeric G protein subunits, Ras, and PPARγ (Li *et al.*, 1995; Garcia-Cardena *et al.*, 1997; Ju *et al.*, 1997; Oka *et al.*, 1997; Song *et al.*, 1997; Feron *et al.*, 1998; Bucci *et al.*, 2000; Bernatchez *et al.*, 2005; Burgermeister *et al.*, 2011; Kraehling *et al.*, 2016). However, other studies based on assessing the structure of CSD/CSDBM interaction suggested that caveolin–protein interactions are rare (Collins *et al.*, 2012).

This article was published online ahead of print in MBoC in Press (http://www.molbiolcell.org/cgi/doi/10.1091/mbc.E19-12-0713) on April 2, 2020.

The authors declare no competing financial interest.

*Address correspondence to: Chinnaswamy Tiruppathi (tiruc@uic.edu); Asrar B. Malik (abmalik@uic.edu).

Abbreviations used: Cav-1, caveolin-1; CFP, cyan fluorescent protein; CSD, Cav-1 scaffold domain; CSDBM, CSD binding motif; 3D-SIM, 3D-structured illumination microscopy; ECs, endothelial cells; Eph, erythropoietin-producing hepatocellular carcinoma; FRET, fluorescence resonance energy transfer; YFP, yellow fluorescent protein.

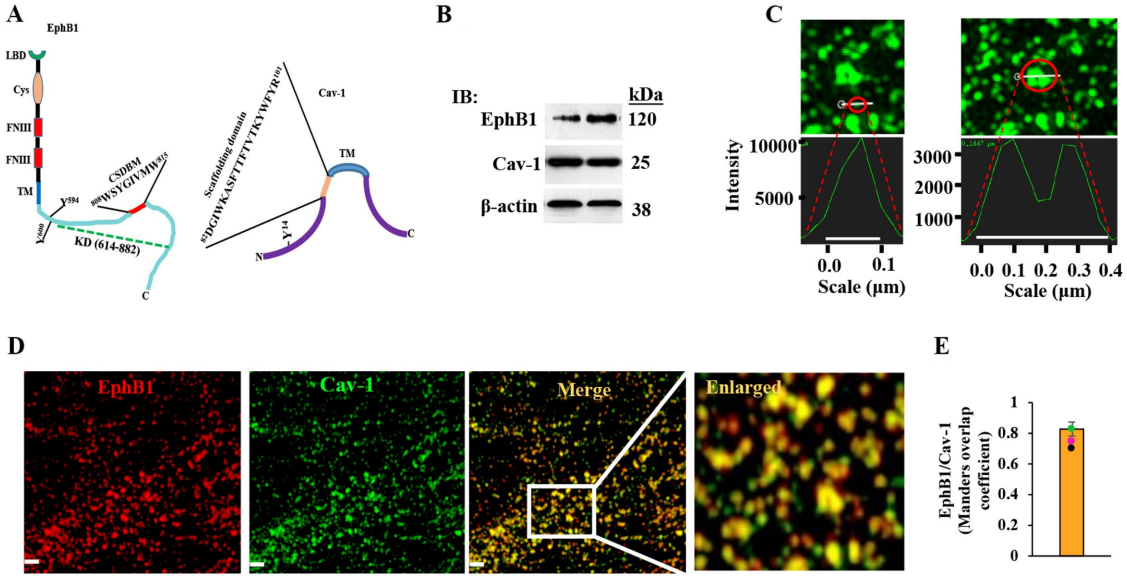

FIGURE 1: Colocalization of EphB1 and caveolin-1 (Cav-1) determined by 3D-structured illumination microscopy. (A) Schematic representation of structural domain features of EphB1 and Cav-1. CSD, Cav-1 scaffold domain; CSDBM, CSD binding motif in EphB1; LBD, ligand-binding domain; Cys, cysteine-rich domain; FNIII, fibronectin-type III repeats; TM, transmembrane domain; KD (dashed green line), EphB1 kinase domain (614–882). (B) Western analysis of human lung microvessel endothelial cells (HLMVECs) showing the expression of EphB1 and Cav-1. (C) HLMVECs stained with antibody specific to Cav-1 were used for 3D-structured illumination microscopy (3D-SIM) imaging. Representative sectional view of single cell plasma membrane image from 3D-SIM showing Cav-1+ve vesicular structures (caveola, 100 nm, left; caveolar clusters, 400 nm, right). (D) HLMVECs stained with antibodies specific to Cav-1 and EphB1 were used for 3D-SIM to assess colocalization of EphB1 with Cav-1. Representative sectional view of single cell plasma membrane image from 3D-SIM showing colocalization of EphB1 with Cav-1. In Merge, a magnified view of the region is shown. Scale bars correspond to 1 μm. (E) Colocalization efficiency of EphB1 and Cav-1 as assessed by Manders overlap coefficient is shown. $N = 4$ cells.

Erythropoietin-producing hepatocellular carcinoma (Eph) receptor tyrosine kinases and their ligands, Ephrins, are expressed in multiple cell types including ECs (Barquilla and Pasquale, 2015; Kania and Klein, 2016). Eph receptors have an important role in regulating neuronal and vascular development, axon guidance, and cell-specific identities (Henkemeyer *et al.*, 1996; Williams *et al.*, 2003; Kuijper et al, 2007; Salvucci and Tosato, 2012). Ephrins also regulate postnatal angiogenesis and vascular integrity (Salvucci *et al.*, 2006; Kuijper *et al.*, 2007; Salvucci and Tosato, 2012; Nikolov *et al.*, 2014; Tosato, 2017) by mechanisms that are not clear. Most Eph receptors also exhibit the conserved CSDBM in their kinase domain indicative of a binding relationship with Cav-1 (Figure 1A; Vihanto *et al.*, 2006; Barquilla and Pasquale, 2015; Kania and Klein, 2016). In a study using CHO cells, EphB1 was shown to bind CSD via its CSDBM (^{808}WSYGIVMW^{815}; Vihanto *et al.*, 2006). Furthermore, knockdown of EphB4 expressed in human umbilical vein ECs reduced Cav-1 phosphorylation on Y14 secondary to EphB4 activation by the ligand Ephrin B2 (Luxan *et al.*, 2019). These findings suggest a potential signaling link between Eph receptors and Cav-1; however, the details of this relationship and their functional significance remain incompletely understood. In the present study, we demonstrated that EphB1/Cav-1 interaction formed a signaling module that was required for the biogenesis of caveolae and function of caveolae in ECs. EphB1-dependent *Src* activation resulting in Cav-1 phosphorylation on Y14 induced caveolae-mediated endocytosis and trafficking.

RESULTS

EphB1 colocalizes with Cav-1 in ECs

We studied the interaction of EphB1 with Cav-1 expressed in human lung microvascular ECs (HLMVECs; Figure 1B). We initially used 3D-structured illumination microscopy (3D-SIM) superresolution microscopy in which the spatial resolution of an ~100-nm structure could be resolved (Wu and Shroff, 2018). We observed heterogeneous vesicular structures ranging from caveola of diameter 100 nm (Figure 1C) to multilobed caveolar rosettes of 400 nm (Figure 1C). EphB1 was predominantly colocalized with Cav-1 positive multilobed caveolar rosettes (Figure 1D). Colocalization as quantified by measuring the Manders overlap coefficient (Manders *et al.*, 1993) showed strong EphB1 with Cav-1 association (Figure 1E).

Autophosphorylation of EphB1 uncouples EphB1 from Cav-1 to induce Y14 Cav-1 phosphorylation

Because EphB1 and Cav-1 colocalized in caveolar microdomains, we next investigated the possibility that EphB1/Cav-1 interaction regulates the canonical Y-14 phosphorylation site of Cav-1 via *Src* activation, a critical mechanism of Cav-1 signaling (Minshall *et al.*, 2000; Shajahan *et al.*, 2004; Zimnicka *et al.*, 2016). Here we added the EphB1 agonist Ephrin B1-Fc, the soluble Ephrin B1 extracellular domain fused to Fc fragment, (Barquilla and Pasquale, 2015; Kania and Klein, 2016), to wild-type (WT) murine lung ECs (from C57BL/6 mice). We observed marked tyrosine phosphorylation of EphB1 post–Ephrin B1-Fc stimulation (Figure 2A). Interestingly, the binding of phosphorylated EphB1 binding to *Src* and phosphorylation of *Src* at Y416 (an indication of *Src* activation) occurred in the same time frame as EphB1 phosphorylation (Figure 2A), a finding consistent with binding of SH2 domain of *Src* to phosphotyrosine on EphB1 responsible for triggering *Src* activation (Vindis *et al.*, 2003). Ephrin B1-Fc stimulation also induced intense phosphorylation of Cav-1 on Y14 site (Figure 2B). Next, using 3D-SIM, we observed marked colocalization of EphB1 with Cav-1 in multilobed caveolar

structures, which was markedly reduced within 5–10 min of adding Ephrin B1-Fc ligand (Figure 2C and Supplemental Figure 1, A and B). These results are consistent with immunoprecipitation (IP) experiments showing that Ephrin B1–induced phosphorylation of EphB1 causes the dissociation of EphB1 from Cav-1, whereas dephosphorylated EphB1 promotes reassociation with Cav-1 (Figure 2A). Because it is possible that other EphB receptors expressed in ECs may also be activated by Ephrin B1, we addressed whether the observed effects of the Ephrin B1 ligand were specific to the EphB1 receptor. Thus, we used the EphB1 selective antagonistic peptide (EphB1-A-pep; Figure 2D; Koolpe *et al.*, 2005; Riedl and Pasquale, 2015), which prevents binding of Ephrin B1 to EphB1 ligand-binding domain, and inhibits EphB1 signaling (Koolpe *et al.*, 2005; Riedl and Pasquale, 2015). HLMVECs treated with EphB1-A-pep prevented Ephrin B1–induced EphB1 autophosphorylation (Figure 2E) as well as *Src* activation (p-Y416; Figure 2F) and phosphorylation of Cav-1 on Y14 as compared with control peptide (Figure 2G), indicating the specificity of Ephrin B1 in activating its cognate receptor EphB1 in ECs.

Ligand Ephrin B1 prevents EphB1/Cav-1 interaction and induces *Src* activation and *Src*-dependent Y14 Cav-1 phosphorylation

To address the role of EphB1/Cav-1 complex in signaling *Src*-dependent Cav-1 phosphorylation, we first coexpressed WT-EphB1-YFP with either WT-Cav-1-CFP or the mutant EphB1$^{\Delta 808\text{-}815}$-YFP with WT-Cav-1-CFP in COS-1 cells, and determined the associations of each pair by 3D-SIM superresolution microscopy. We observed the colocalization of WT-EphB1-YFP with WT-Cav-1-CFP in caveolar rosette structures (Figure 3B and Supplemental Figure 2, A and B) and markedly reduced colocalization of WT-EphB1-YFP with WT-Cav-1-CFP upon Ephrin B1-Fc addition (Figure 3B and Supplemental Figure 2, A and B). Interestingly, the expression of mutant EphB1$^{\Delta 808\text{-}815}$ in which CSDBM was deleted prevented the colocalization EphB1 with WT-Cav-1-CFP (Figure 3C and Supplemental Figure 2, A and B), indicating that CSDBM per se of EphB1 was required for EphB1 interaction with Cav-1.

We next carried out fluorescence resonance energy transfer (FRET) studies to assess further the interaction between EphB1 and Cav-1. Here we coexpressed WT-EphB1-YFP with either WT-Cav-1-CFP or the mutant EphB1$^{\Delta 808\text{-}815}$-YFP with WT-Cav-1-CFP in COS-1 cells. We observed fourfold greater FRET intensity in the cells coexpressing WT-EphB1-YFP and WT- Cav-1-CFP than the cells expressing EphB1$^{\Delta 808\text{-}815}$-YPF and WT-Cav-1-CFP (Figure 3D). Stimulation of cells coexpressing WT-EphB1-YFP and WT-Cav-1-CFP with Ephrin B1-Fc showed markedly reduced FRET intensity (Figure 3D), whereas cells coexpressing EphB1$^{\Delta 808\text{-}815}$-YPF and WT-Cav-1-CFP showed no response (Figure 3D), further supporting the essential role of Ephrin B1 ligand binding to EphB1 in causing the dissociation of EphB1 from Cav-1.

As EphB1 autophosphorylation on Y600 was to mediate *Src* binding and activation (Vindis *et al.*, 2003), we next determined whether EphB1 CSDBM binding to Cav-1 was required for the ligand Ephrin B1–mediated *Src* activation secondary to autophosphorylation of EphB1 at Y600. Here we coexpressed WT-EphB1-YFP with either WT-Cav-1-CFP, mutant EphB1$^{\Delta 808\text{-}815}$-YFP with WT-Cav-1-CFP, or mutant EphB1^{Y600F}-YFP with WT-Cav-1-CFP in COS-1 cells (Figure 3, E and F). By IP analysis using anti–EphB1-specific antibody, we observed interaction between WT-EphB1 and WT-Cav-1 (Figure 3E), whereas CSDBM-deleted mutant EphB1 (EphB1$^{\Delta 808\text{-}815}$) failed to interact with WT-Cav-1 (Figure 3E). Interestingly, mutant EphB1^{Y600F}-YFP binding to WT-Cav-1-CFP was not altered (Figure 3E), indicating that phosphorylation of EphB1 was not a requirement for EphB1/Cav-1 interaction. Next we used anti-GFP antibody for immunoprecipitation, and immunoprecipitated samples were used to assess phosphorylation of EphB1, *Src*, and Cav-1. We observed autophosphorylation of EphB1 and phosphorylation of both *Src* on Y-416 and Cav-1 on Y-14 in WT-EphB1 and WT-Cav-1 coexpressing cells, which were increased in both cases by Ephrin B1-Fc ligand (Figure 3F). In EphB1$^{\Delta 808\text{-}815}$ and WT-Cav-1 coexpressing cells, however, we observed basal as well as Ephrin B1–induced phosphorylation of EphB1, *Src* and Cav-1 were blocked (Figure 3F). Similar results were obtained in mutant EphB1^{Y600F} and WT-Cav-1 coexpressing cells (Figure 3F). These results collectively support the notion that the binding of CSD with CSDBM in EphB1 and autophosphorylation of EphB1 on Y600 are required for EphB1-mediated *Src* activation, and Cav-1 phosphorylation on Y-14.

EphB1/Cav-1 interaction regulates caveolae biogenesis

We next studied EphB1-deleted mice (*EphB1*$^{-/-}$) and mice expressing EphB1-tc (EphB1-βgal fusion receptor lacking the tyrosine kinase and C-terminal domains). Western blot analysis of lung tissue and isolated lung ECs showed the absence of EphB1 expression in *EphB1*$^{-/-}$ mice (Supplemental Figure 3, A and B) and the expression of EphB1-βgal fusion receptor in EphB1-tc mice (Supplemental Figure 3, A and B). Immunostaining of lung sections from EphB1-tc mice with antibodies to β-gal and vWF (an EC marker) showed β-gal expression in blood vessels (Supplemental Figure 3C). Using *EphB1*$^{-/-}$ mice to study whether EphB1 affected Cav-1 expression in vivo, we found that Cav-1 protein expression was markedly reduced in *EphB1*$^{-/-}$ mice as compared with WT (Figure 4A). Interestingly, decreased Cav-1 protein expression was not associated with reduced Cav-1 mRNA in *EphB1*$^{-/-}$ mice (Figure 4B), indicating that EphB1 posttranscriptionally regulated Cav- 1 expression. As Cav-1 is known to be ubiquitinated and degraded via a proteasomal pathway (Hayer *et al.*, 2010; Bakhshi *et al.*, 2013), we assessed the possibility of ubiquitination of Cav-1 in ECs of *EphB1*$^{-/-}$ mice, and showed increased Cav-1 ubiquitination in ECs from *EphB1*$^{-/-}$ mice as compared with WT ECs (Figure 4C). In intestinal epithelial cells, siRNA-mediated suppression of lipid raft-associated protein flotillin-1 promoted Cav-1 degradation via lysosomal pathway (Vassilieva *et al.*, 2009). Because Cav-1 expression was markedly reduced in EphB1-deficient mice, we address the possibility that EphB1 may regulate Cav-1 expression through suppressing flotillin-1 in ECs. We observed that flotillin-1 expression in lung tissue and ECs was not different between WT and *EphB1*$^{-/-}$ mice (Figure 4D), suggesting that EphB1 direct binding to Cav-1 prevents Cav-1 degradation in ECs and that flotillin-1 was not involved. Next we assessed the expression of the caveolar coat proteins cavin-1 and -2 (Hansen *et al.*, 2013; Kovtun *et al.*, 2015). It has been shown that cavin-2 is required for caveolar structure formation in murine lung ECs (Hansen *et al.*, 2013). We observed that cavin-1 expression was not different between the genotypes, but cavin-2 expression was increased in *EphB1*$^{-/-}$ mice (Figure 4E), suggesting that cavin-2 accumulates in ECs in the absence of EphB1, perhaps because of the defective formation of caveolae in ECs of *EphB1*$^{-/-}$ mice (Figure 5). We next carried out an ultrastructural analysis and observed markedly impaired caveolar morphogenesis in lung and heart microvascular endothelia of *EphB1*$^{-/-}$ mice (Figure 5, A and B). The number of caveolae was significantly reduced in ECs of lungs (Figure 5A, right panel; 4.2 ± 0.2/μm in WT mice vs. 1.3 ± 0.2/μm *EphB1*$^{-/-}$ mice) and hearts (5.4 ± 0.3/μm in *EphB1*$^{+/+}$ mice vs. 2.6 ± 0.3/μm *EphB1*$^{-/-}$ mice; Figure 5B, right panel). However, there were no differences in caveolar shapes in these ECs (Figure 5, A and B) and in interendothelial

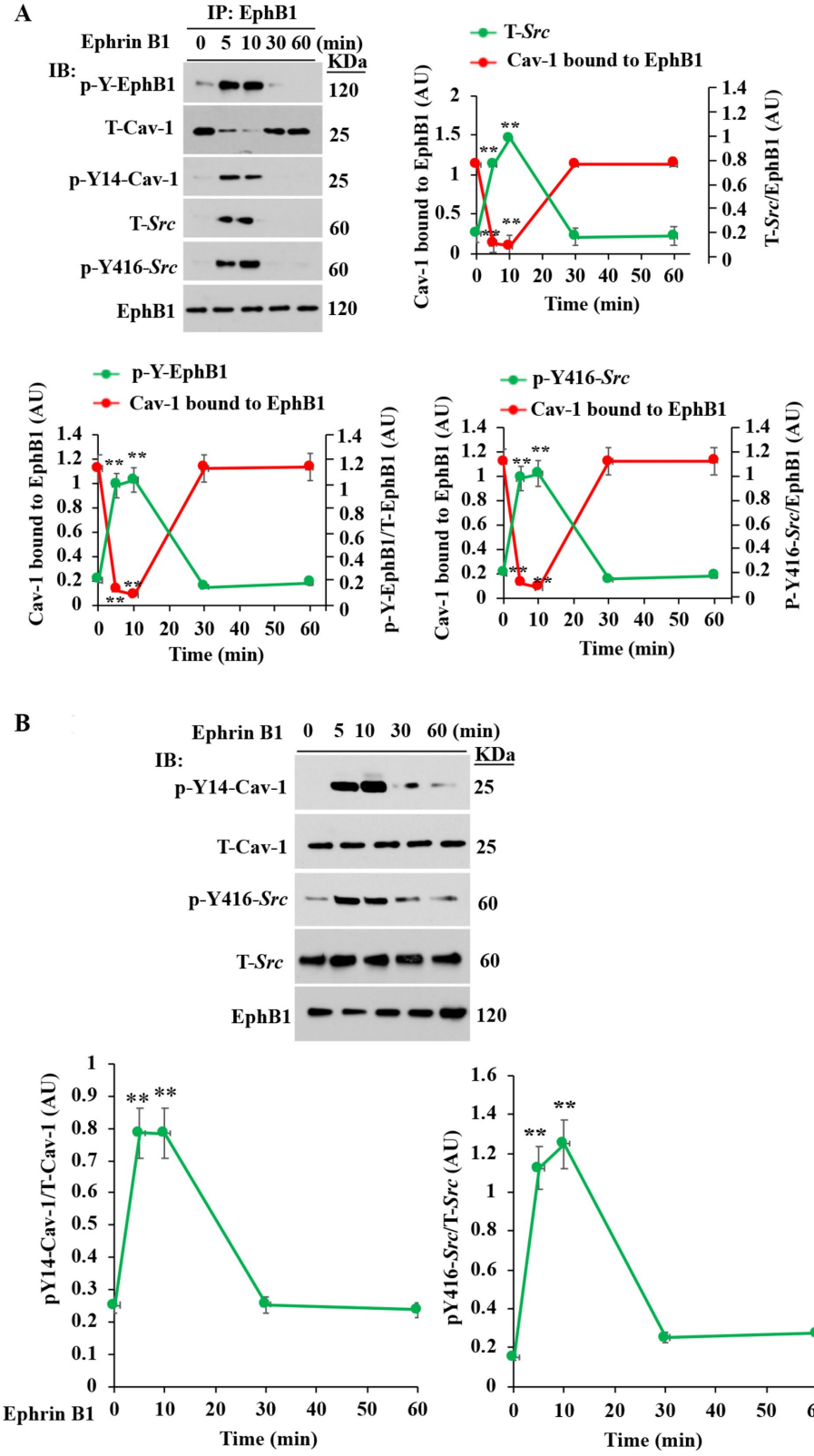

junctions (Supplemental Figure 4). 3D-SIM superresolution microscopy demonstrated that the number of caveolae (defined as Cav-1–positive structures) was also markedly reduced in ECs of *EphB1*$^{-/-}$ mice, and caveolar rosette-like structures in ECs formed by fusion of multiple caveolae were not seen in ECs from *EphB1*$^{-/-}$ mice as compared with WT ECs (Figure 5C).

EphB1-dependent Y-14 phosphorylation of Cav-1 regulates caveolae endocytosis and endothelial permeability

To address next whether EphB1 regulates caveolae-mediated endocytosis, we compared responses in ECs from *EphB1*$^{-/-}$ and *Cav-1*$^{-/-}$ mice. Ephrin B1 induced time-dependent increases in phosphorylation of *Src* on Y-416 and Y-14 Cav-1 in WT ECs, whereas these responses were prevented in ECs from *Cav-1*$^{-/-}$ mice (Figure 6, A and B). In ECs from *EphB1*$^{-/-}$ mice, we observed that Ephrin B1–induced phosphorylation on *Src* Y-416 and Cav-1 Y-14 were also blocked (Figure 6, C and D). We also assessed using ECs from *EphB1*$^{-/-}$ and

FIGURE 2: (A–C) Ephrin B1–induced autophosphorylation of EphB1 causes EphB1 binding to *Src*, phosphorylation of *Src* on Y-416, and Cav-1 on Y-14 to uncouple EphB1 from Cav-1. (A, B) ECs from WT mice were serum starved for 2 h and then exposed to Ephrin B1-Fc (1 μg/ml) for different times up to 60 min for immunoprecipitation followed by immunoblot (IB). In A, cell lysates were immunoprecipitated (IP-ed) with anti-EphB1 pAb and the IP-ed proteins were used for IB with specific antibodies indicated. In B, total cell lysates were used for IB. Results shown are representative of three experiments. **, $p < 0.001$, compared with basal. (C) WT ECs serum starved for 2 h and then exposed to Ephrin B1-Fc (1μg/ml) for different times up to 60 min, and immunostained with antibodies specific to EphB1 and Cav-1, were used for 3D-SIM imaging. Sectional images are of single cell plasma membrane from 3D-SIM showing changes in colocalization of EphB1 with Cav-1 at baseline and following stimulation with the ligand Ephrin B1-Fc. In Merge, a magnified view of the region is indicated. Scale bars correspond to 1 μm. The right panel shows the EphB1 and Cav-1 colocalization efficiency assessed by Manders overlap coefficient. $N = 5$ cells/group; *, $p < 0.05$, compared with basal. (D–G) EphB1-specific antagonistic peptide prevents Ephrin B1–induced autophosphorylation of EphB1, *Src* activation, and phosphorylation of Cav-1 on Y-14. (D) Sequences of EphB1 antagonistic peptide (EphB1-A-Pep) and control peptide (Control Pep) are shown. (E–G) HLMVECs incubated in serum-free condition for 2 h at 37°C were treated with EphB1-Ap-pep or control peptide (Control Pep) for 30 min. Cells were then exposed to EphrinB1 (EphrinB1-Fc; 1 μg/ml) for 10 min at 37°C. In E, cell lysates immunoprecipitated with anti-EphB1 pAb and blotted with anti-phosphotyrosine mAb to determine phosphorylation of EphB1. In F, total cell lysates were used to determine phosphorylation of *Src* at Y416 to assess *Src* activation. In G, total cell lysates were used to determine phosphorylation of Cav-1 on Y-14. (E–G) Blots shown are representative of three separate experiments. **, $p < 0.001$; control vs. EphB1-A-pep.

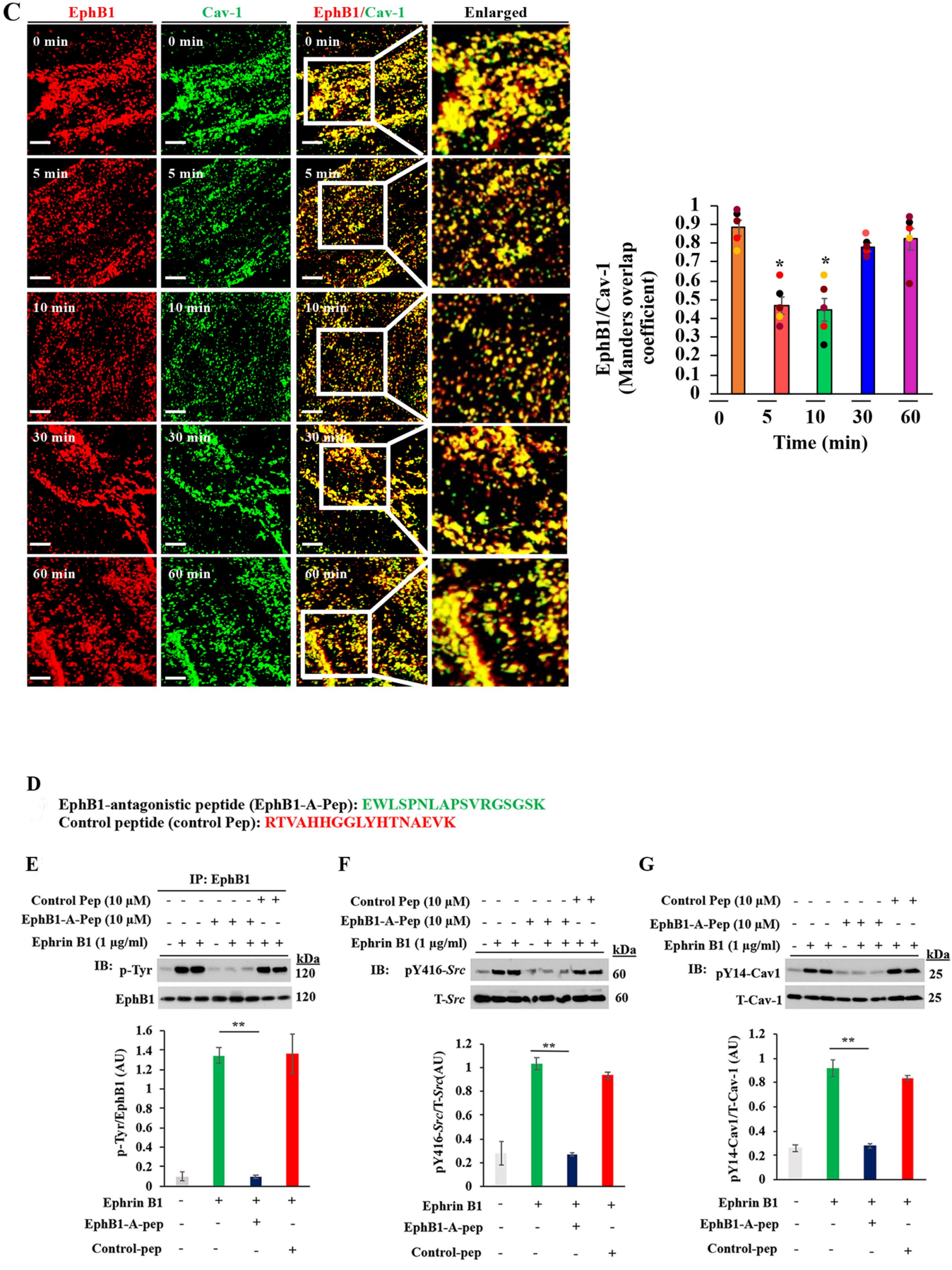

FIGURE 2: Continued.

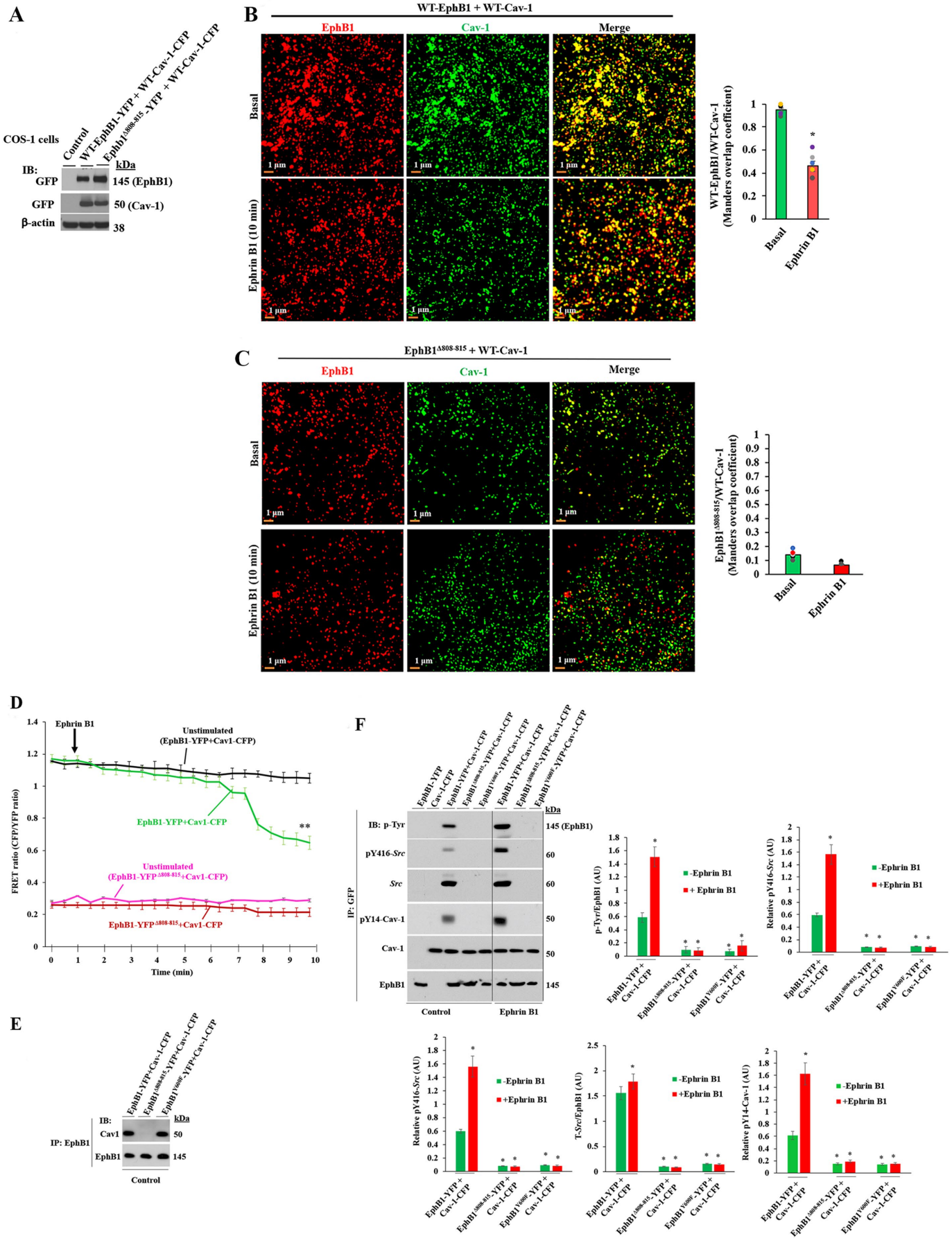
A
COS-1 cells
Control
WT-EphB1-YFP + WT-Cav-1-CFP
EphB1Δ808-815-YFP + WT-Cav-1-CFP
IB:
kDa
GFP
145 (EphB1)
GFP
50 (Cav-1)
β-actin
38
B
WT-EphB1 + WT-Cav-1
EphB1
Cav-1
Merge
Basal
Ephrin B1 (10 min)
1 μm
WT-EphB1/WT-Cav-1 (Manders overlap coefficient)
Basal
Ephrin B1
C
EphB1Δ808-815 + WT-Cav-1
EphB1
Cav-1
Merge
Basal
Ephrin B1 (10 min)
1 μm
EphB1Δ808-815/WT-Cav-1 (Manders overlap coefficient)
Basal
Ephrin B1
D
Ephrin B1
Unstimulated (EphB1-YFP+Cav1-CFP)
EphB1-YFP+Cav1-CFP
**
Unstimulated (EphB1-YFPΔ808-815+Cav1-CFP)
EphB1-YFPΔ808-815+Cav1-CFP
FRET ratio (CFP/YFP ratio)
Time (min)
E
EphB1-YFP+Cav-1-CFP
EphB1Δ808-815-YFP+Cav-1-CFP
EphB1V600F-YFP+Cav-1-CFP
IB:
kDa
IP: EphB1
Cav1
50
EphB1
145
Control
F
EphB1-YFP
Cav-1-CFP
EphB1-YFP+Cav-1-CFP
EphB1Δ808-815-YFP+Cav-1-CFP
EphB1V600F-YFP+Cav-1-CFP
EphB1-YFP+Cav1-CFP
EphB1Δ808-815-YFP+Cav1-CFP
EphB1V600F-YFP+Cav1-CFP
kDa
IB: p-Tyr
145 (EphB1)
pY416-Src
60
Src
60
pY14-Cav-1
50
Cav-1
50
EphB1
145
IP: GFP
Control
Ephrin B1
p-Tyr/EphB1 (AU)
-Ephrin B1
+Ephrin B1
Relative pY416-Src (AU)
Relative pY14-Cav-1 (AU)
T-Src/EphB1 (AU)

Cav-1$^{-/-}$ mice whether EphB1/Cav-1 interaction was required for signaling caveolae-mediated endocytosis. Caveolae endocytosis was determined by quantifying the uptake of tracer albumin Alexa Fluor–594–labeled bovine serum albumin tracer (Alexa Fluor–594 BSA; John *et al.*, 2003; Zimnicka *et al.*, 2016). ECs were incubated with serum-free medium for 2 h followed by the addition of Ephrin B1-Fc ligand (1 µg/ml) in the medium containing 100 µg/ml albumin tracer plus 2 mg/ml unlabeled albumin. Analysis of single cell 3D images showed albumin internalization in WT ECs as early as 5 min after tracer addition. We observed 16 ± 3 particles/cell with maximum uptake of 850 ± 14 particles/cell attained at 60 min (Figure 7A and Table 1). Numerous Cav-1–positive caveolae were seen in ECs of WT mice (Figure 7A), whereas ECs from *EphB1*$^{-/-}$ mice showed fourfold reduction in albumin tracer internalization (in WT ECs 850 ± 14 particles/cell at 60 min vs. in *EphB1*$^{-/-}$ ECs 216 ± 16 particles/cell; Figure 7, A and B, and Table 1). The uptake of albumin was also inhibited in *Cav-1*$^{-/-}$ ECs (Figure 7, C and D, and Table 1) similar to ECs from *EphB1*$^{-/-}$ mice. To next address in vivo relevance of EphB1/Cav-1 interaction in mediating transendothelial albumin permeability, we used tracer ^{125}I-albumin (Tiruppathi *et al.*, 2008). *EphB1*$^{-/-}$ mice showed marked reduction in endothelial ^{125}I-albumin permeability as compared with WT (Figure 7E), and furthermore, treatment with anti-EphB1 pAb receptor blocking antibody significantly reduced ^{125}I-albumin permeability in vivo (Figure 7F).

DISCUSSION

We describe a functionally important interaction in ECs between the receptor tyrosine kinase EphB1 with the canonical caveolar protein Cav-1 in regulating the activation of *Src* and *Src*-mediated phosphorylation of Cav-1 on Y14. *Src* signaling induced by the uncoupling of EphB1/Cav-1 interaction mediated caveolar endocytosis and trafficking. We showed that CSDBM of EphB1 binds via the scaffold domain of Cav-1 (CSD), and thus constitutively masks the EphB1 kinase domain and holds *Src* in abeyance. However, activation of EphB1 by its native ligand Ephrin B1 uncoupled EphB1 from Cav-1, exposing the EphB1 kinase domain to activate *Src* and thereby induce *Src*-dependent phosphorylation of Y-14 Cav-1, the phosphoactive site on Cav-1 responsible for caveolae-mediated endocytosis (Minshall *et al.*, 2000; Shajahan *et al.*, 2004; Zimnicka *et al.*, 2016).

Multiple signaling proteins have been shown to bind CSD (Li *et al.*, 1995; Garcia-Cardena *et al.*, 1997; Ju *et al.*, 1997; Oka *et al.*, 1997; Song *et al.*, 1997; Feron *et al.*, 1998; Bucci *et al.*, 2000; Bernatchez *et al.*, 2005; Burgermeister *et al.*, 2011; Kraehling *et al.*, 2016). However, on the basis of structural and bioinformatic analysis, it appears that physical interactions between CSD and CSDBM are less common than previously believed (Collins *et al.*, 2012). CSDBM is buried in the membrane making it inaccessible to bind many CSD-containing proteins (Collins *et al.*, 2012; Ariotti *et al.*, 2015). Thus far, only *Src* kinases (*Src, Fyn*) and dynamin-2 were shown to definitively bind nonphosphorylated Cav-1, whereas TRAF2 was shown to bind to Y-14 phosphorylated Cav-1 (Jung *et al.*, 2018). Our results based on biochemical, genetic, superresolution microscopy and FRET analysis showed clear evidence of interaction of EphB1 with CSD of nonphosphorylated Cav-1 via the EphB1 CSDBM.

Ephrin ligation of Eph receptors mediates conformational changes in Eph receptors important for the activation of *Src* tyrosine kinase (Barquilla and Pasquale, 2015; Kania and Klein, 2016). Phosphorylation of the conserved Y-600 in the cytoplasmic juxta-membrane region of EphB1 both recruited and activated *Src* (Vindis *et al.*, 2003). We observed by immunoprecipitation, 3D-SIM superresolution imaging, and FRET analysis that the ligand Ephrin B1 induced dissociation of the receptor EphB1 from Cav-1. This uncoupling unmasked EphB1 kinase domain (which contains the CSDBM) to autophosphorylate EphB1 at Y-600 and induce *Src* kinase activation and Y-14 Cav-1 phosphorylation. We observed that coexpression of mutant EphB1^{Y600F} with WT-Cav-1 failed to phosphorylate *Src* on Y416 as well as Cav-1 on Y-14. These findings show that *Src* activation is a key signaling switch responsible for EphB1/Cav-1 dissociation and phosphorylation of Y-14 Cav-1, the requisite signal for caveolae-mediated endocytosis (Minshall *et al.*, 2000; Shajahan *et al.*, 2004; Zimnicka *et al.*, 2016). An important unknown, however, is how a conformation change induced by Ephrin B1 binding to EphB1 leads to *Src* phosphorylation and downstream signaling.

Deletion of Cav-1 prevented the formation of caveolae (Drab *et al.*, 2001; Schubert *et al.*, 2002; Cheng and Nichols, 2016) indicating that Cav-1 expression is essential for caveolae biogenesis in

FIGURE 3: (A-D) EphB1 colocalization with caveolin-1 (Cav-1) scaffold binding domain (CSD) assessed by 3D-structured illumination microscopy (3D-SIM) and FRET. (A) Western analysis of COS-1 cells transfected with WT-EphB1-YFP (WT-EphB1 C-terminus fused with YFP), WT-Cav-1-CFP (WT-Cav-1 C-terminus fused with CFP), and EphB1Δ808-815-YFP. (B) Sectional image of COS-1 cell expressing WT-EphB1 plus WT-Cav-1 using 3D-SIM showing CSDBM of EphB1 interacts with WT-Cav-1. *Top panel*, representative unstimulated cell sectional view of 3D image. *Bottom panel*, representative COS-1 cell sectional view of a 3D image showing the effect of Ephrin B1-Fc (1 µg/ml) stimulation, which caused EphB1 dissociation from Cav-1. *Right panel*, EphB1 and Cav-1 colocalization efficiency assessed by Manders overlap coefficient (MOC). $N = 4$ cells/group; *, $p < 0.05$, compared with basal. (C) Sectional images of COS-1 cell expressing EphB1$^{\Delta 808\text{-}815}$ plus WT-Cav-1 using 3D-SIM showing an absence of interaction between CSDBM-deleted EphB1 (EphB1$^{\Delta 808\text{-}815}$) and WT-Cav-1. *Top panel*, control. *Bottom panel*, stimulated with Ephrin B1-Fc (1 µg/ml). *Right panel*, colocalization efficiency between EphB1$^{\Delta 808\text{-}815}$ and Cav-1 assessed by MOC. (D) Live-cell FRET measurements in COS-1 cells showing dissociation of EphB1 from Cav-1 after challenging with Ephrin B1. CFP/YFP ratio before and after challenging cells with the ligand Ephrin B1 (Ephrin B1-Fc; 1 µg/ ml) are shown. Results shown are mean ± SE of three separate experiments. **, $p < 0.001$, compared with WT-EphB1 + WT-Cav-1 control (green) or EphB1$^{\Delta 808\text{-}815}$ + WT-Cav-1 (red) exposed to Ephrin B1. (E, F) Binding of CSDBM of EphB1 to CSD and EphB1 phosphorylation on Y^{600} are required for *Src* activation and Cav-1 phosphorylation on Y14. (E) WT-EphB1-YFP + WT-Cav-1-CFP, EphB1$^{\Delta 808\text{-}815}$-YFP+ WT-Cav-1-CFP, or EphB1^{Y600F}-YFP + WT-Cav-1-CFP expressing Cos-1 cells IP-ed with anti-EphB1 pAb and immunoblot with anti-Cav-1 pAb or anti-EphB1 mAb. (F) WT-EphB1-YFP + WT-Cav-1-CFP, EphB1$^{\Delta 808\text{-}815}$-YFP+ WT-Cav-1-CFP, or EphB1^{Y600F}-YFP + WT-Cav-1-CFP expressing Cos-1 cells were stimulated with or without EphrinB1-Fc (1 µg/ml) for 10 min. Cell lysates were IP-ed with anti-GFP mAb (anti-GFP mAb immunoprecipitates both YFP- tagged EphB1 and CFP-tagged Cav-1) and were blotted with indicated antibodies. Results shown are representative of three experiments. *, $p < 0.01$.

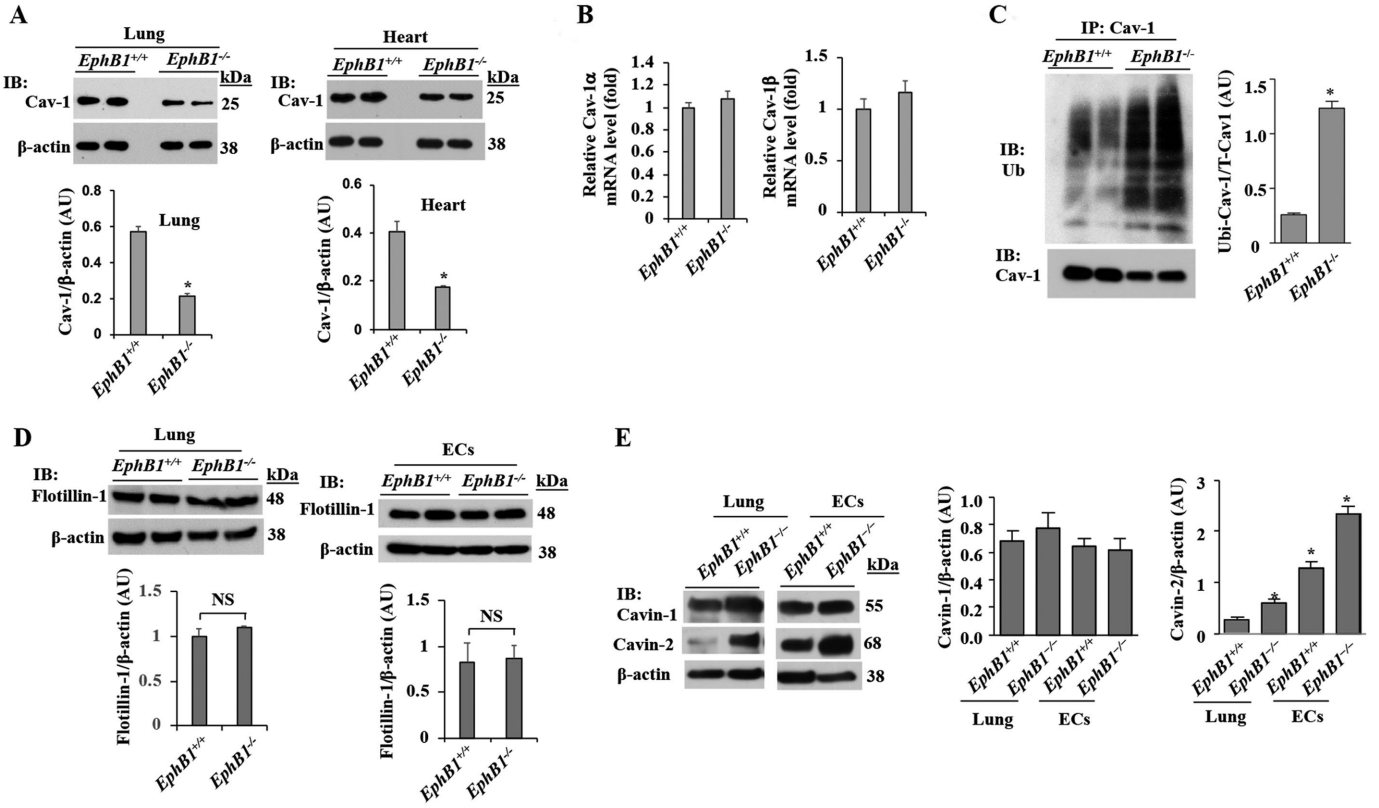

FIGURE 4: EphB1 regulates the expression of Cav-1. (A) Lung and heart tissues from WT (*EphB1*$^{+/+}$) and EphB1 knockout (*EphB1*$^{-/-}$) mice were used for Western blotting to determine Cav-1 expression. $n = 5$ mice per group; unpaired *t* test. *, $p < 0.05$. (B) EphB1 deficiency did not alter Cav-1 mRNA expression. Quantitative real-time PCR was performed utilizing total RNA from lung tissue of WT and *EphB1*$^{-/-}$ mice to determine mRNA expression for Cav-1α and Cav-1β isoforms. (C) EphB1 deficiency induced Cav-1 degradation via ubiquitination. Freshly isolated lung ECs from WT and *EphB1*$^{-/-}$ mice were IP-ed with anti–Cav-1 mAb and blotted with anti–pan-ubiquitin (Ubi) pAb. $n = 5$ mice per genotype used for EC isolation; unpaired *t* test. *, $p < 0.05$. (D) EphB1 deficiency did not alter flotillin-1 expression. Lung tissue and lung ECs (ECs) from WT (*EphB1*$^{+/+}$) and *EphB1*$^{-/-}$ mice were used to determine flotillin-1 expression by Western analysis. $n = 4$ mice per group; three separate EC preparations were used. Unpaired *t* test. NS, not significant. (E) Expression of caveolar coat proteins Cavin-2 but not Cavin-1 was increased in *EphB1*$^{-/-}$ mice. Lung tissue and lung ECs (ECs) from WT (*EphB1*$^{+/+}$) and *EphB1*$^{-/-}$ mice were used to determine Cavin-1 and Cavin-2 by Western analysis. $n = 5$ mice per group; three separate EC preparations were used. Unpaired *t* test. *, $p < 0.05$.

ECs. CSD is required for caveolae biogenesis because caveolae also did not form upon deletion of CSD (Ariotti *et al.*, 2015). In the present study, we observed that deletion of CSDBM on EphB1 disrupted the formation of caveolae. That both Cav-1 and EphB1 induced similar caveolae biogenesis defects suggests that EphB1/Cav-1 interaction through CSD/CSDBM is a critical determinant of the formation of caveolae. An important question is why other proteins interacting with CSD of Cav-1 such as eNOS did not influence the genesis of caveolae (Predescu *et al.*, 2005). We showed that the transmembrane EphB1 was basally associated with Cav-1 at the plasma membrane unlike eNOS (Song *et al.*, 1997; Bucci *et al.*, 2000). Thus, constitutive association of Cav-1 with EphB1 in the plasmalemma may stabilize Cav-1 and facilitate the formation of homo-oligomers or hetero-oligomers with Cav-2, and hence contribute to caveolae formation (Parton and del Pozo, 2013; Busija *et al.*, 2017).

We demonstrated that *Src*-dependent Cav-1 phosphorylation on Y-14 was essential for signaling caveolae-mediated endocytosis in ECs (Minshall *et al.*, 2000; Shajahan *et al.*, 2004; Zimnicka *et al.*, 2016). Using ECs from *EphB1*$^{-/-}$ mice, we observed that Ephrin B1 failed to induce *Src* activation and Cav-1 phosphorylation. Furthermore, caveolae-mediated endocytosis was also abrogated in ECs of *EphB1*$^{-/-}$ mice. These findings together show that EphB1 signaling is a critical upstream regulator of Cav-1–mediated caveolar endocytosis and trafficking.

There are multiple reports of internalization of plasma albumin in caveolae and caveolar trafficking across the endothelium by a specialized transport mechanism (Ghitescu *et al.*, 1986; Schnitzer and Oh, 1994). However, the normally high plasma albumin concentration of 3–4 g% suggests that such a mechanism should be fully saturated, hence the role of caveolae in trafficking macromolecular cargo such as albumin across endothelium has remained unsettled and controversial (Collins *et al.*, 2012; Cheng and Nichols, 2016; Jung *et al.*, 2018). In the endothelium of the developing vasculature, Ephrin B2 was shown to regulate vascular endothelial growth factor receptor endocytosis (Sawamiphak *et al.*, 2010; Wang *et al.*, 2010). Furthermore, Ephrin B2 signaling-mediated distribution of platelet-derived growth factor receptor β (PDGFRβ) to the Cav-1–positive membrane microdomains suppressed PDGFRβ-mediated downstream signaling in vascular smooth muscle cells (Nakayama *et al.*, 2013). The findings of these studies circumstantially raise the possibility that Ephrin signaling in endothelium could modulate endocytosis of caveolae by localizing the Eph receptor tyrosine kinases in the caveolar microdomains.

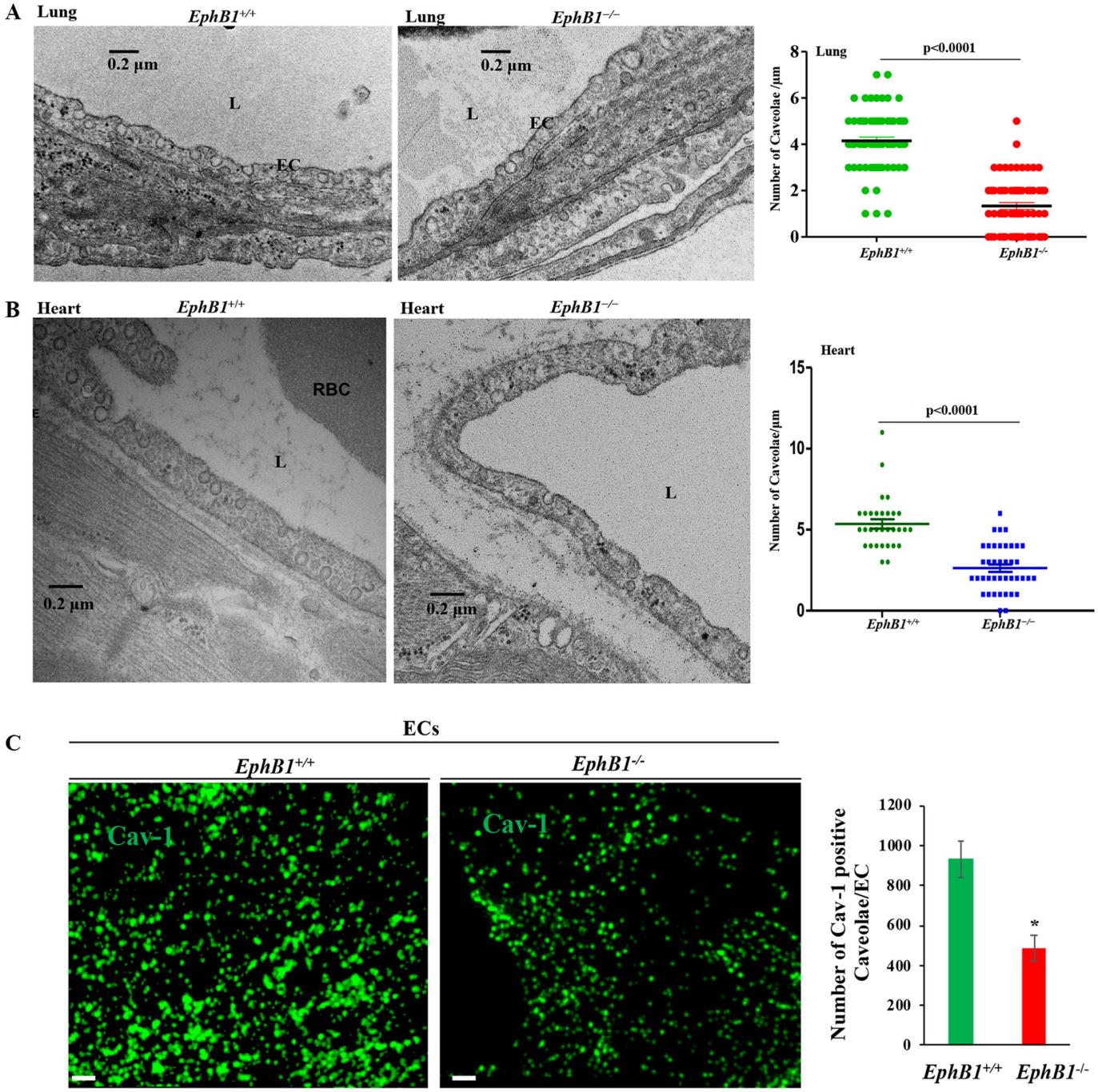

FIGURE 5: EphB1 is required for caveolae morphogenesis in endothelial cells. (A) Electron micrograph showing reduced caveolae number in lung endothelia of *EphB1*$^{-/-}$ mice with morphometric data in right panel. Caveolae open at the cell surface were counted per micrometer of endothelial luminal plasma membrane. Multiple electron micrographs were used for counting caveolae; *EphB1*$^{+/+}$ (WT) lungs, $n = 67$; *EphB1*$^{-/-}$ lungs, $n = 66$. L, lumen; EC, endothelium; $p < 0.0001$ vs. *EphB1*$^{+/+}$. (B) Electron micrograph showing reduced caveolae number in heart endothelia of *EphB1*$^{-/-}$ mice with morphometric data in right panel. *EphB1*$^{+/+}$ (WT) hearts, $n = 31$; *EphB1*$^{-/-}$ hearts, $n = 40$. L, lumen; $p < 0.0001$ vs. *EphB1*$^{+/+}$. (C) 3D-SIM superresolution microscopy image showing reduced number of Cav-1+ve structures in *EphB1*$^{-/-}$-ECs. ECs from WT and *EphB1*$^{-/-}$ mice were stained with anti–Cav-1 pAb and used to obtain images by 3D-SIM superresolution microscopy. Representative sectional view of single cell plasma membrane image from 3D-SIM superresolution microscopy showing Cav-1+ve vesicles in lung endothelial cells from *EphB1*$^{+/+}$ and *EphB1*$^{-/-}$ mice. $n = 5$ cells per genotype; *, $p < 0.05$.

In the present study, we demonstrated that soluble Ephrin B1 binding to EphB1/Cav-1 complex induced *Src* phosphorylation on Y-14 Cav-1 and activated caveolae-mediated endocytosis and the caveolar transport machinery. Studies have shown that soluble Ephrins can function as ligands for distant cell localized Eph receptors (Wykosky *et al.*, 2008; Lagares *et al.*, 2017). Therefore, it is possible

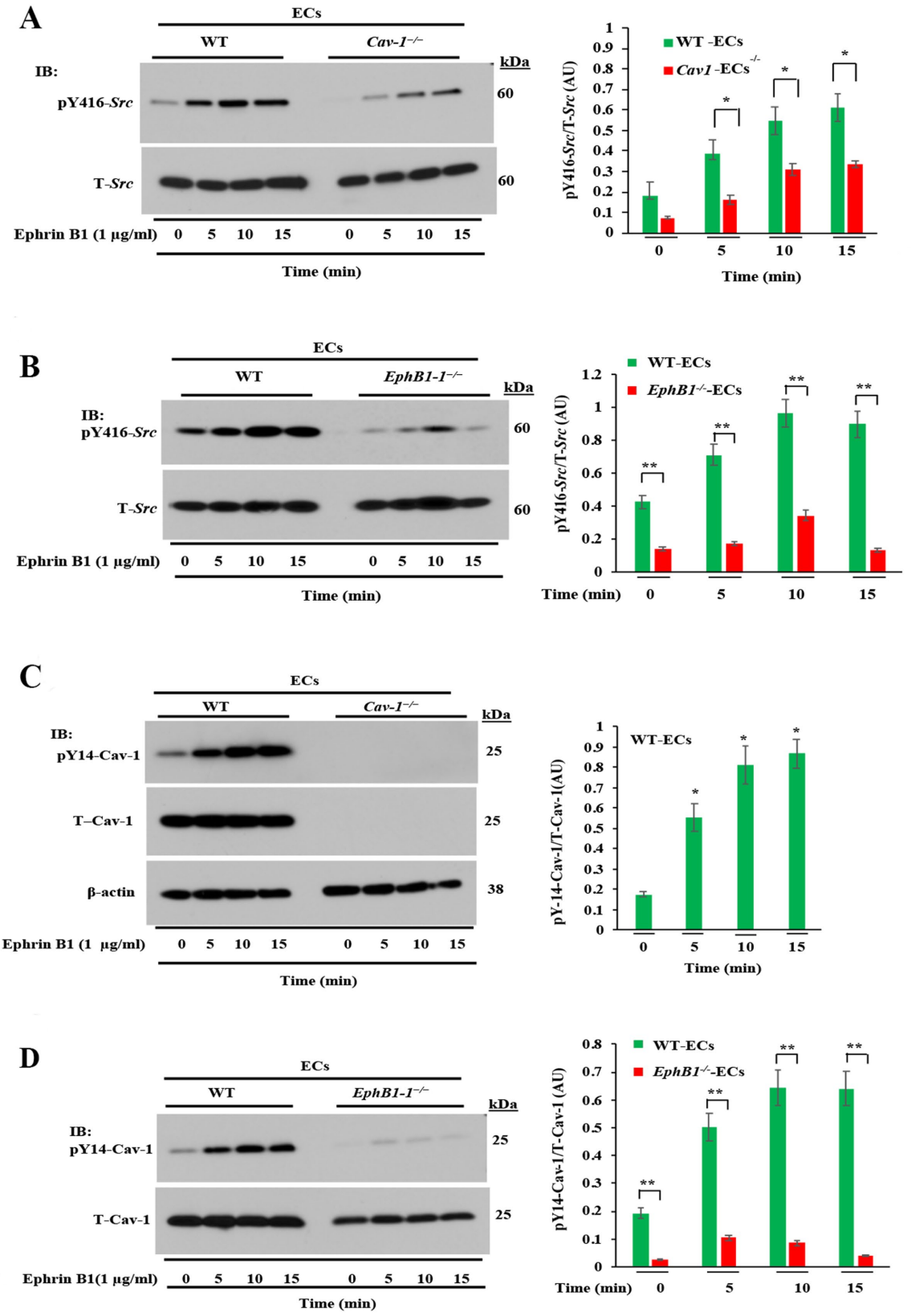

FIGURE 6: EphB1/Cav-1 interaction is required for Y-416 phosphorylation on *Src* (A, C) and Cav-1 phosphorylation on Y-14 (B, D). ECs from *Cav-1*$^{+/+}$ (WT), *Cav-1*$^{-/-}$, *EphB1*$^{+/+}$ (WT), and *EphB1*$^{-/-}$ mice exposed to EphrinB1 (EphrinB1-Fc; 1 µg/ml) for the indicated times were used for immunoblotting to determine phosphorylation of *Src* on Y-416 (left panels) and Cav-1 on Y-14 (pY14-Cav-1; right panels). Blots shown are representative of three to four separate experiments. Values are shown as mean ± SE. *, $p < 0.05$; **, $p < 0.001$; compared with controls; WT-LECs (lung endothelial cells) vs. *Cav-1*$^{-/-}$ or *EphB1*$^{-/-}$.

that soluble Ephrins in the circulation may activate EphB1/Cav-1 signaling complex in endothelial cell surface. If this is the case, the question arises as to how soluble Ephrins are generated in the circulation. One possible mechanism could be through metalloprotease-mediated shedding of Ephrin B1 from platelets and Ephrin B2 from ECs (Prevost *et al.*, 2004, 2005; Lagares *et al.*, 2017; Montague *et al.*, 2018). Another mechanism could involve release of Ephrin B2 containing extracellular vesicles (exosomes or microparticles) by ECs (Gong *et al.*, 2016; Pasquale, 2016). Thus, EphB1 ligation by Ephrins B1/2 generated in plasma (Salvucci *et al.*, 2006; Barquilla and Pasquale, 2015; Gong *et al.*, 2016) may itself activate caveolar trafficking via *Src*-mediated Y-14 phosphorylation of Cav-1. This concept needs testing but it is consistent with the observation that *EphB1*$^{-/-}$ mice showed markedly reduced transendothelial ^{125}I-albumin permeability as compared with WT mice.

MATERIAL AND METHODS

Antibodies and other reagents

Anti–Cav-1 rabbit polyclonal (cat. #610059), anti–phos-Y14-Cav-1 mouse monoclonal (cat. #611338), and anti–flotillin-1 mouse monoclonal (cat. #610821) antibodies were from BD Transduction (San Jose, CA). Anti-*Src* rabbit monoclonal (cat. #21235), anti–phos-Y416 *Src* rabbit polyclonal (cat. #21015), and pan anti-ubiquitin polyclonal (cat. #3933S) antibodies were obtained from Cell Signaling (Danvers, MA). Anti–cavin-1 (PTRF) pAb (cat. #18892-1) and anti–Cavin-2 (SDPR) pAb (cat. #12339-1) were from Protein-Tech group (Chicago, IL). Chicken polyclonal β-galactosidase antibody (cat. #ab9361) was from Abcam. Rabbit polyclonal von Willebrand factor antibody (cat. #AB7356) obtained from Millipore Corp. Rabbit polyclonal antibody against EphB1 sequence (AA 528-541, DDDYKSELREQLPL; anti-EphB1 pAb) was custom produced by Sigma-Aldrich (St. Louis, MO). Anti-EphB1 mouse monoclonal against EphB1 sequence (AA 528-541, DDDYKSELREQLPL) was custom made by GenScript. EphB1 panning (receptor antagonistic) peptide (EWLSPNLAPSVRGSGSK) and scrambled control peptide (RTVAHHGGLYHTNAEVK) were synthesized by GenScript. PCR primers were custom synthesized from Integrated DNA technologies. Mouse recombinant EphrinB1-Fc chimera (cat. #E0653-200UG) and BSA (cat. #05470-1G) with purity >98% were from Sigma. Alexa Fluor–594 BSA (cat. #A13101), Alexa Fluor–488 chicken anti-rabbit (cat. #A21441), and Alexa Fluor–647 goat anti-mouse (cat. #A21236) were from Life Technologies (Carlsbad, CA). Tracer ^{125}I-human serum albumin was from AnazaoHealth (Tampa, FL).

Mice

EphB1-deficient (*EphB1*$^{-/-}$) and EphB1-tc (EphB1-βgal fusion receptor lacking the tyrosine kinase and C-terminal domains) mice generated on a CD1 background (Henkemeyer *et al.*, 1996; Williams *et al.*, 2003). Caveolin-1–deficient (*Cav-1*$^{-/-}$) mice on a C57BL/6J background (Schubert *et al.*, 2002) were from Jackson Labs. Age-matched *EphB1*$^{+/+}$, *EphB1*$^{-/-}$, *EphB1-tc*, *Cav-1*$^{+/+}$, and *Cav-1*$^{-/-}$ littermates were used for all experiments. All mice were housed in the University of Illinois Animal Care Pathogen Free Facility in accordance with institutional guidelines and guidelines of the U.S. National Institutes of Health. Veterinary care of these animals and related animal experiments was approved by the University of Illinois Animal Resources Center.

Quantitative real-time PCR

Total RNA was isolated from lung tissue and reverse transcribed with oligo(dt) primers and SuperScript reverse transcriptase (Invitrogen). The cDNA obtained was mixed with SYBR Green PCR mix (AB Applied Biosystems). An ABI prism 7000 was used for quantitative PCR. GAPDH expression served as an internal control. The following primers were used: mouse Cav-1α forward, 5′-AATACGTAGACTCCGAGGGACA-3′, and reverse, 5′-GACCACGTCGTCGTTGAGAT-3′; mouse Cav-1β, forward, 5′-TGAACTTTTCTTCCCACCGCT-3′, and reverse, 5′-TCAAAGTCAATCTTGACCACGTC-3′; GAPDH forward, 5′-ACCCAGAAGACTGTGGATGG-3′, and reverse, 5′-CACATTGGGGGTAGGAACAC-3′.

Expression constructs and transfection

C-terminal CFP-tagged Cav-1 was prepared as described previously (Zimnicka *et al.*, 2016). pcDNA3 vector expressing mouse EphB1 C-terminal YFP-tagged (WT-EphB1-YFP), C-terminal YFP-tagged EphB1$^{\Delta 808\text{-}815}$ (EphB1$^{\Delta 808\text{-}815}$-YFP), and C-terminal YFP-tagged EphB1^{Y600F} (EphB1^{Y600F}-YFP) were custom prepared by GenScript. DNA sequencing was performed to verify all the expression constructs sequences. COS-1 cells plated on 60-mm dishes at 60% confluency were transfected with WT-Cav-1-CFP (1 µg) plus WT-EphB1-YPF (2.5 µg), WT-Cav-1-CFP (1 µg) plus EphB1$^{\Delta 808\text{-}815}$-YFP (2.5 µg), or WT-Cav-1 (1 µg) plus EphB1^{Y600F}-YFP (2.5 µg using Superfect transfection reagent (cat. #301305; Qiagen). Media was replaced 6 h after transfection with fresh DMEM media containing 10% fetal bovine serum. After 72 h, cells were harvested and lysed in radioimmunoprecipitation assay buffer containing protease and phosphatase inhibitor cocktails. For 3D-SIM imaging experiments, 24 h after transfection, cells were plated on high-tolerance coverslips (pcs-170-1818; MatTek), and at 72 h, cells were used for experiments.

Live-cell FRET imaging

Live-cell FRET imaging was performed as described previously (Zimnicka *et al.*, 2016).

ECs

HLMVECs and endothelial growth media-2 (EGM-2) were purchased from Lonza (Walkersville, MD). Lung ECs from mice were isolated with mAb to the adhesion molecule CD31 (PECAM-1; Tiruppathi *et al.*, 2002).

Immunoblotting

ECs were washed three times with phosphate-buffered saline (PBS) at 4°C and lysed in lysis buffer (50 mM Tris-HCl, pH, 7.5, 150 mM NaCl, 1 mM EGTA, 1% Triton X-100, 0.25% sodium deoxycholate, 0.1% SDS, 10 µM orthovanadate, and protease-inhibitor mixture; Tiruppathi *et al.*, 2014). Mouse tissues were homogenized in lysis buffer (Tiruppathi *et al.*, 2014). EC lysates or tissue homogenates were resolved by SDS–PAGE on a 4–15% gradient separating gel under reducing conditions and transferred to a Duralose membrane. Membranes were blocked with 5% dry milk in TBST (10 mM Tris-HCl, pH 7.5, 150 mM NaCl, and 0.05% Tween-20) for 1 h at RT and then incubated with the indicated primary antibody diluted in blocking buffer overnight at 4°C. For phospho-specific blots, membranes were incubated overnight at 4°C with the primary antibody diluted in TBST containing 5% BSA. Next, membranes were washed three times and incubated with appropriate HRP-conjugated secondary antibody. Protein bands were detected by enhanced chemiluminescence.

Immunostaining

Cells grown on high-tolerance coverslips (pcs-170-1818; MatTek) were incubated with serum-free medium (5 mM HEPES/HBSS, pH 7.4)

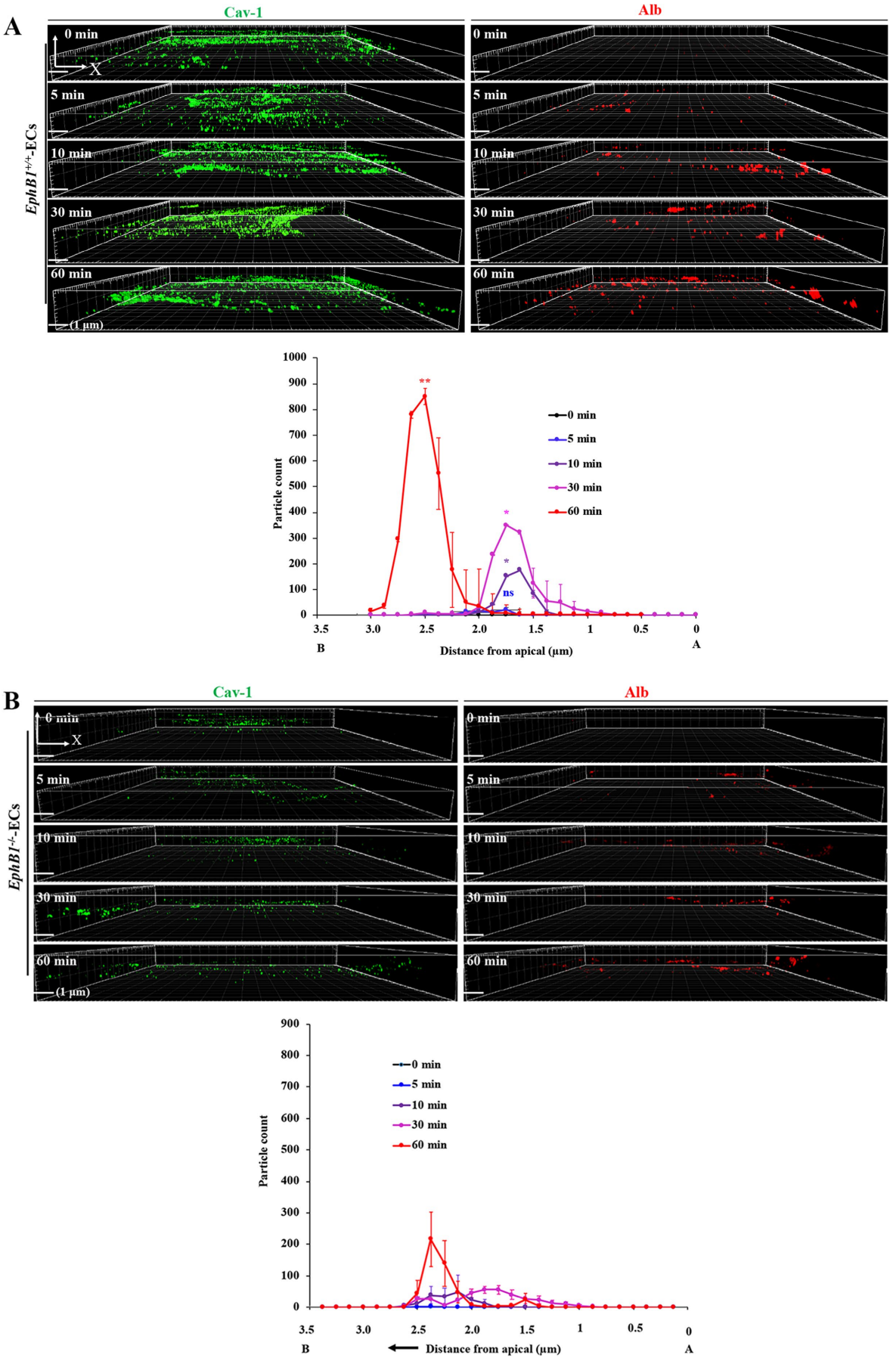

FIGURE 7: Continues.

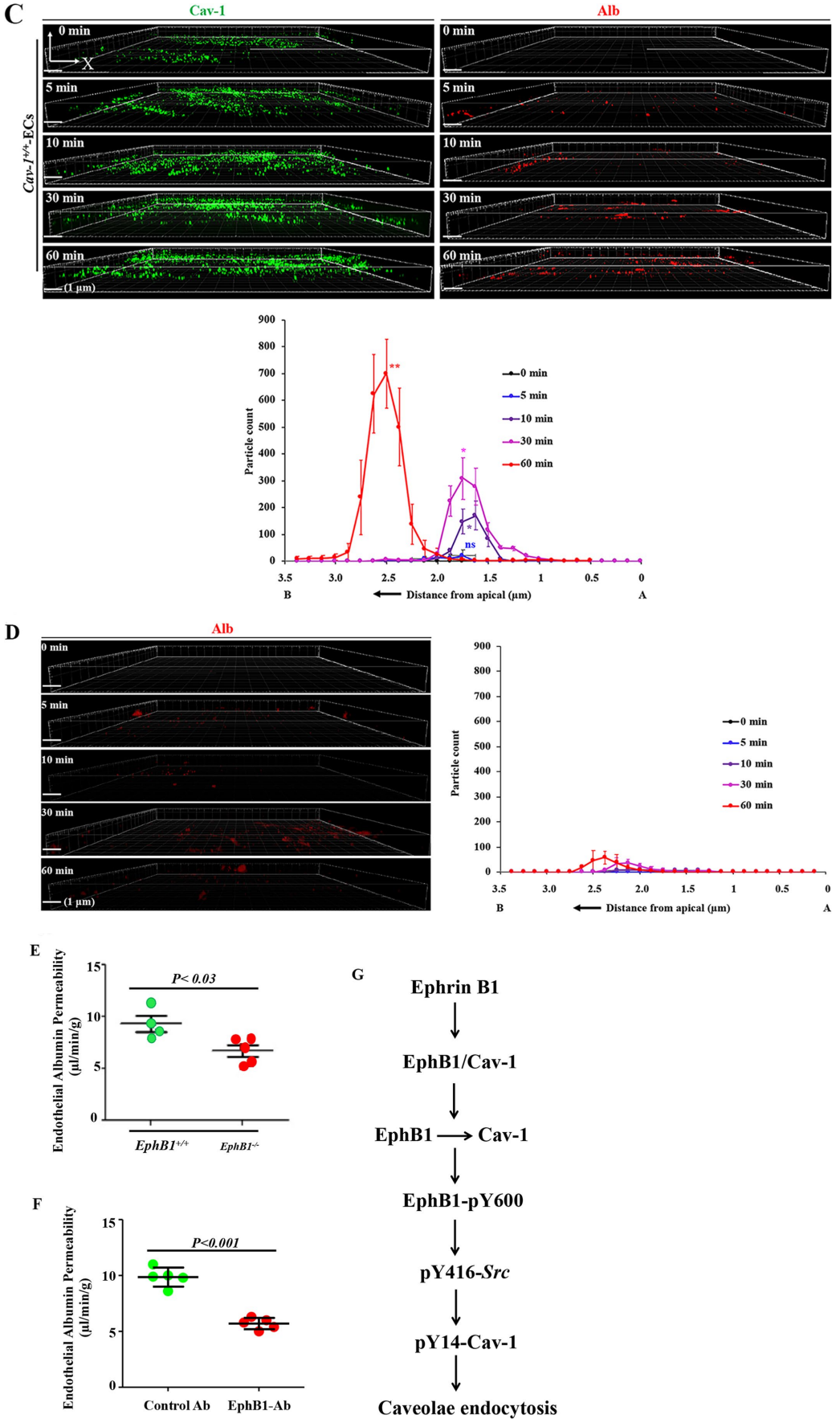

FIGURE 7: Continued.

FIGURE 7: (A–D) EphB1 is required for caveolae-mediated endocytosis and albumin permeability. (A) WT ECs (EphB1$^{+/+}$); (B) *EphB1*$^{-/-}$-ECs; (C) Cav-1$^{+/+}$-ECs; (D) *Cav-1*$^{-/-}$-ECs. (A–D) Representative 3D images of single cell labeled with Cav-1 (green) and albumin tracer (red) tracking from apical and basal aspects of ECs are shown. Images in each 3D-SIM data set were processed using the Particle Analysis function in Image J software. Results show the time course of Ephrin B1-Fc (1 μg/ml) –induced albumin internalization and passage from apical to basal aspects of ECs (A–C, bottom panels, and D, left panel). (A) apical side; (B) basolateral side. *, $p < 0.05$; **, $p < 0.001$; compared with 0 min. Transendothelial permeability of tracer ^{125}I-albumin measured in wild-type (*EphB1*$^{+/+}$) and *EphB1*$^{-/-}$ mice. $n = 5$ per group (E). Anti-EphB1 pAb (5 μg/ml) prevents transendothelial permeability of tracer ^{125}I-albumin in WT mice similarly compared with control antibody (F). $n = 5$ per group (*EphB1*$^{+/+}$). (G) Model for EphB1/Cav-1 signaling in mediating caveolae endocytosis and albumin permeability in ECs.

Time (min)	*EphB1*$^{+/+}$	*EphB1*$^{-/-}$	*Cav-1*$^{+/+}$	*Cav-1*$^{-/-}$
0	0 ± 0	0 ± 0	0 ± 0	0 ± 0
5	16 ± 3	2 ± 2**	9 ± 2	0 ± 0**
10	175 ± 14	37 ± 13**	170 ± 13	9 ± 7**
30	350 ± 8	55 ± 13**	308 ± 9	35 ± 15**
60	850 ± 14	216 ± 16**	699 ± 17	58 ± 15**

Values are mean ± SE; $n = 5$/cells/genotype.
**, $p < 0.001$; *EphB1*$^{+/+}$-ECs vs. *EphB1*$^{-/-}$-ECs; **, $p < 0.001$; *Cav-1*$^{+/+}$-ECs vs. *Cav-1*$^{-/-}$-ECs.

TABLE 1: Albumin tracer particles/EC determined by 3D-SIM superresolution microscopy.

for 2 h and stimulated with Ephrin B1-Fc (1 μg/ml) for indicated time periods. Cells were washed, fixed with 3% paraformaldehyde (PFA) in Hank's balanced salt solution (HBSS), permeabilized with 0.1% Tween-20 in 5 mM HEPES/HBSS, pH 7.4, and blocked with 5% human serum diluted with 5 mM HEPES/HBSS, pH 7.4 (blocking buffer) for 2 h at room temperature. After blocking, cells were incubated with primary antibodies (1 μg/ ml) anti- EphB1 mouse mAb or anti-Cav-1 rabbit mAb in blocking buffer overnight at 4°C. Cells were washed and incubated with 1 μg/ml secondary antibody Alexa Fluor–647 goat anti-mouse and Alexa Fluor–488 chicken anti-rabbit for 1 h. After washing, coverslips were mounted on microscope slides with ProLong Gold antifade reagent (Invitrogen).

Immunoprecipitation

Cell lysate (150 μg protein) was subjected to immunoprecipitation. Each sample was incubated overnight with 1 μg/ml of the indicated antibody at 4°C. The next day, protein A/G beads were added to the sample and incubated for 1 h at 4°C. Immunoprecipitates were then washed three times with wash buffer (Tris-buffered saline containing 0.05% Triton X-100, 1 mM Na_3VO_4, 1 mM NaF, 2 μg/ml leupeptin, 2 μg/ml pepstatin A, 2 μg/ml aprotinin, and 44 μg/ml phenylmethylsulfonyl fluoride). Immunoprecipitated proteins were used for immunoblotting.

3D-SIM

All 3D-SIM imaging was performed on a DeltaVision OMX SR system (GE) equipped with an Olympus 60×/1.42 NA objective and refractive index matched immersion oil ($n = 1.516$–1.518) at room temperature. Full-frame structure illuminated image sequences were taken at 125 nm *Z*-axis sections for multiple *Z* positions; the same exposure and excitation parameters were undertaken to avoid pixel saturation and maintain the validity of comparison across samples. 3D-SIM images were reconstructed using Softworx (Applied Precision) offline using a Wiener filter coefficient of 0.001. Reconstructed 3D-SIM data was further processed by Imaris software (Bitplane; Zurich, Switzerland). To ensure colocalization accuracy, all color channels in the 3D-SIM system have been aligned using standard samples. The image in each 3D data set was processed using the Particle Analysis function in ImageJ to quantify the number and intensity of specific protein particles in each *Z* section.

Transmission electron microscopy

WT and *EphB1*$^{-/-}$ mice were anesthetized with ketamine/xylazine (100 mg kg/5 mg kg) by intraperitoneal injection. Harvested organs were perfused with HBSS containing EM fixative (2% glutaraldehyde, 3% PFA, 0.1 M sodium cacodylate, pH 7.2). Tissue blocks (1 × 2 mm) were prepared fixed in fresh fixative, rinsed in 0.1 M sodium cacodylate, postfixed in 1% OsO_4 in 0.1 M sodium cacodylate, rinsed, stained en bloc with Kellenberger's uranyl acetate in water, dehydrated through graded ethanol, and embedded in LX-112 resin using propylene oxide. Ultrathin sections of 20–40 nm were cut and mounted on grids, stained with uranyl acetate and lead citrate, and examined under a Joel 1220 electron microscope (Stan *et al.*, 2012).

Caveolae endocytosis assay

Caveolae-mediated endocytosis of tracer albumin was measured as described (Minshall *et al.*, 2000; Shajahan *et al.*, 2004). Briefly, ECs grown on high-tolerance coverslips (pcs- 170-1818; MatTek) were washed, incubated for 2 h in serum-free medium, followed by Alexa Fluor 594–conjugated albumin (0.1 mg/ml Alexa Fluor 594–BSA mixed into 2 mg/ml nonfluorescent BSA) in 5 mM HEPES-buffered HBSS at 37°C for up to 60 min (Minshall *et al.*, 2000; Shajahan *et al.*, 2004). After this period of incubation, cells were washed, fixed with 3% PFA in HBSS, permeabilized with 0.1% Tween-20 in 5 mM HEPES/HBSS, pH 7.4, and blocked with 5% human serum diluted with 5 mM HEPES/HBSS, pH 7.4 for 2 h at RT. After blocking, cells were incubated with anti–Cav-1 rabbit mAb (1 μg/ml) in blocking buffer overnight at 4°C. Cells were washed and incubated with 1 μg/ml secondary antibody Alexa Fluor 488 chicken anti-rabbit for 1 h. After washing, coverslips were mounted on microscope slides with ProLong Gold antifade reagent (Invitrogen).

Endothelial permeability assay

We determined transendothelial permeability in lung vessels in WT or *EphB1*$^{-/-}$ mice were anesthetized using 2.5% sevoflurane in room air, and 2 μCi of ^{125}I-labeled albumin tracer injected intravenously according to an approved animal protocol. At 30 min after tracer injection, a 100-μl blood sample was withdrawn from a vein to determine blood tracer counts. Organs were then cleared of circulating tracer by whole-body perfusion via the right heart using RPMI supplemented with 3% unlabeled albumin and lungs were excised and counted for γ-radioactivity. Transendothelial albumin permeability was calculated in ml/min/g dry tissue from blood and tissues counts, and values were normalized to tissue dry weight as described (Tiruppathi et al 2008). To study the effects of the anti-EphB1 pAb on transendothelial albumin permeability, we used the method

as described by us (Vogel *et al.*, 2000; Tiruppathi *et al.*, 2002). Murine lungs were perfused via the pulmonary artery with RPMI solution containing 3% unlabeled albumin (2 ml/min, 37°C). All preparations underwent a 20-min equilibration perfusion, and then received control Ab or anti-EphB1 pAb via a side-arm of the pulmonary artery cannula to achieve a final perfusate concentration of 5 µg/ml each. The ^{125}I-albumin tracer was infused via a separate side-arm for a 30-min period. A perfusate sample was collected to determine blood tracer counts and then washed out for 6 min, a period sufficient to reduce effluent counts to background levels. Lungs were counted for gamma radioactivity, and transendothelial albumin permeability was quantified in units of ml/min/g dry lung.

Statistical analysis

Results were analyzed by unpaired two-tailed Student's *t* test. Differences in mean values were considered significant at p value <0.05.

ACKNOWLEDGMENTS

This work was supported by National Institutes of Health Grants no. R01 HL-128359, no. R01 GM-117028, no. R01 HL-122157, and no. P01 HL-060678.

REFERENCES

Ariotti N, Rae J, Leneva N, Ferguson C, Loo D, Okano S, Hill MM, Walser P, Collins BM, Parton RG (2015). Molecular characterization of caveolin-induced membrane curvature. J Biol Chem 290, 24875–24890.

Bakhshi FR, Mao M, Shajahan AN, Piegeler T, Chen Z, Chernaya O, Sharma T, Elliott WM, Szulcek R, Bogaard HJ, *et al.* (2013). Nitrosation-dependent caveolin 1 phosphorylation, ubiquitination, and degradation and its association with idiopathic pulmonary arterial hypertension. Pulm Circ 3, 816–830.

Barquilla A, Pasquale EB (2015). Eph receptors and ephrins: therapeutic opportunities. Annu Rev Pharmacol Toxicol 55, 465–487.

Bernatchez PN, Bauer PM, Yu J, Prendergast JS, He P, Sessa WC (2005). Dissecting the molecular control of endothelial NO synthase by caveolin-1 using cell-permeable peptide. Proc Natl Acad Sci USA 102, 761–766.

Bucci M, Gratton JP, Rudic RD, Acevedo L, Roviezzo F, Cirino G, Sessa WC (2000). *In vivo* delivery of the caveolin-1 scaffold domain inhibits nitric oxide synthesis and reduces inflammation. Nat Med 6, 1362–1367.

Burgermeister E, Friedrich T, Hitkova I, Regel I, Einwächter H, Zimmermann W, Röcken C, Perren A, Wright MB, Schmid RM, Seger R, Ebert MP (2011). The Ras inhibitors caveolin-1 and docking protein 1 activate peroxisome proliferator-activated receptor γ through spatial relocalization at helix 7 of its ligand-binding domain. Mol Cell Biol 31, 3497–3510.

Busija A, Patel RHH, Insel PA (2017). Caveolins and cavins in trafficking, maturation, and degradation of caveolae: implications for cell physiology. Am J Physiol Cell Physiol 312, C459–C477.

Cheng JPX, Nichols BJ (2016). Caveolae: one function or many? J Cell Sci 26, 177–189.

Collins BM, Davis MJ, Hancock JF, Parton RG (2012). Structure-based reassessment of the caveolin signaling model: do caveolae regulate signaling through caveolin-protein interactions? Dev Cell 23, 11–20.

Drab M, Verkade P, Elger M, Kasper M, Lohn M, Lauterbach B, Menne J, Lindschau C, Mende F, Luft FC, *et al.* (2001). Loss of caveolae, vascular dysfunction, and pulmonary defects in caveolin-1 gene-disrupted mice. Science 293, 2449–2452.

Feron O, Dessy C, Opel DJ, Arstall MA, Kelly RA, Michel T (1998). Modulation of the endothelial nitric-oxide synthase-caveolin interaction in cardiac myocytes. Implications for the autonomic regulation of heart rate. J Biol Chem 273, 30249–30254.

Frank PG, Pavlides S, Lisanti MP (2009). Caveolae and transcytosis in endothelial cells: role in atherosclerosis. Cell Tissue Res 335, 41–47.

García-Cardeña GP, Martasek BS, Masters PM, Skidd J, Couet J, Li S, Lisanti MP, Sessa WC (1997). Dissecting the interaction between nitric oxide synthase (NOS) and caveolin. Functional significance of the NOS caveolin binding domain in vivo. J Biol Chem 272, 25437–25440.

Ghitescu L, Fixman A, Simionescu M, Simionescu N (1986). Specific binding sites for albumin restricted to plasmalemmal vesicles of continuous capillary endothelium: receptor-mediated transcytosis. J Cell Biol 102, 1304–1311.

Gong J, Korner R, Gaitanos L, Klein R (2016). Exosomes mediate cell contact-independent ephrin-Eph signaling during axon guidance. J Cell Biol 214, 35–44.

Hansen CG, Shvets E, Howard G, Riento K, Nichols BJ (2013). Deletion of cavin genes reveals tissue- specific mechanisms for morphogenesis of endothelial caveolae. Nat Commun 4, 1831.

Hayer A, Stoeber M, Ritz D, Engl S, Meyer HH, Helenius A (2010). Caveolin-1 is ubiquitinated and targeted to intralumenal vesicles in endolysosomes for degradation. J Cell Biol 191, 615–629.

Henkemeyer M, Orioli D, Henderson JT, Saxton TM, Roder J, Pawson T, Klein R (1996). Nuk controls pathfinding of commissural axons in the mammalian central nervous system. Cell 86, 35–46.

John TA, Vogel SM, Tiruppathi C, Malik AB, Minshall RD (2003). Quantitative analysis of albumin uptake and transport in the rat microvessel endothelial monolayer. Am J Physiol Lung Cell Mol Physiol 284, L187–L196.

Ju H, Zou R, Venema VJ, Venema RC (1997). Direct interaction of endothelial nitric-oxide synthase and caveolin- 1 inhibits synthase activity. J Biol Chem 272, 18522–18525.

Jung W, Sierecki E, Bastiani M, O'Carroll A, Alexandrov K, Rae J, Johnston W, Hunter DJB, Ferguson C, Gambin Y, *et al.* (2018). Cell-free formation and interactome analysis of caveolae. J Cell Biol 217, 2141–2165.

Kania A, Klein R (2016). Mechanisms of ephrin-Eph signalling in development, physiology and disease. Nat Rev Mol Cell Biol 17, 240–256.

Koolpe M, Burgess R, Dail M, Pasquale EB (2005). EphB receptor-binding peptides identified by phage display enable design of an antagonist with ephrin-like affinity. J Biol Chem 280, 17301–17311.

Kovtun O, Tillu VA, Ariotti N, Parton RG, Collins BM (2015). Cavin family proteins and the assembly of caveolae. J Cell Sci 128, 1269–1278.

Kraehling JR, Hao Z, Lee MY, Vinyard DJ, Velazquez H, Liu X, Stan RV, Brudvig GW, Sessa WC (2016). Uncoupling caveolae from intracellular signaling in vivo. Circ Res 118, 48–55.

Kuijper S, Turner CJ, Adams RH (2007). Regulation of angiogenesis by Eph-ephrin interactions. Trends Cardiovasc Med 17, 145–151.

Lagares D, Ghassemi-Kakroodi P, Tremblay C, Santos A, Probst CK, Franklin A, Santos DM, Grasberger P, Ahluwalia N, Montesi SB, *et al.* (2017). ADAM10-mediated ephrin-B2 shedding promotes myofibroblast activation and organ fibrosis. Nat Med 23, 1405–1415.

Li S, Okamoto T, Chun M, Sargiacomo M, Casanova JE, Hansen SH, Nishimoto I, Lisanti MP (1995). Evidence for a regulated interaction between heterotrimeric G proteins and caveolin. J Biol Chem 270, 15693–156701.

Luxán G, Stewen J, Díaz N, Kato K, Maney SK, Aravamudhan A, Berkenfeld F, Nagelmann N, Drexler HC, Zeuschner D, *et al.* (2019) Endothelial EphB4 maintains vascular integrity and transport function in adult heart. elife 8, e45863.

Manders EMM, Verbeek FJ, Aten JA (1993). Measurement of colocalization of objects in dual-color confocal images. J Microsc Oxford 169, 375–382.

Minshall RD, Tiruppathi C, Vogel SM, Niles WD, Gilchrist A, Hamm HE, Malik AB (2000). Endothelial cell-surface gp60 activates vesicle formation and trafficking via G(i)-coupled Src kinase signaling pathway. J Cell Biol 150, 1057–1070.

Montague SJ, Andrews RK, Gardiner EE (2018). Mechanisms of receptor shedding in platelets. Blood 132, 2535–2545.

Nakayama A, Nakayama M, Turner CJ, Höing S, Lepore JJ, Adams RH (2013). Ephrin-B2 controls PDGFRβ internalization and signaling. Genes Dev 27, 2576–2589.

Nikolov DB, Xu K, Himanen JP (2014). Homotypic receptor-receptor interactions regulating Eph signaling. Cell Adh Migr 8, 360–365.

Oka N, Yamamoto M, Schwencke C, Kawabe J, Ebina T, Ohno S, Couet J, Lisanti MP, Ishikawa Y (1997). Caveolin interaction with protein kinase C. Isoenzyme-dependent regulation of kinase activity by the caveolin scaffolding domain peptide. J Biol Chem 272, 33416–33421.

Palade GE (1953). Fine structure of blood capillaries. J Appl Phys 24, 1424.

Pasquale EB (2016). Exosomes expand the sphere of influence of Eph receptors and ephrins. J Cell Biol 214, 5–7.

Parton RG, del Pozo MA (2013). Caveolae as plasma membrane sensors, protectors and organizers. Nat Rev Mol Cell Biol 14, 98–112.

Predescu D, Palade GE (1993). Plasmalemmal vesicles represent the large pore system of continuous microvascular endothelium. Am J Physiol 265, H725–H733.

Predescu SA, Predescu DN, Malik AB (2007). Molecular determinants of endothelial transcytosis and their role in endothelial permeability. Am J Physiol Lung Cell Mol Physiol 293, L823–L842.

Predescu D, Predescu S, Shimizu J, Miyawaki-Shimizu K, Malik AB (2005). Constitutive eNOS-derived nitric oxide is a determinant of endothelial junctional integrity. Am J Physiol Lung Cell Mol Physiol 289, L371–L381.
Predescu D, Vogel SM, Malik AB (2004). Functional and morphological studies of protein transcytosis in continuous endothelia. Am J Physiol Lung Cell Mol Physiol 287, L895–L901.
Prévost N, Woulfe DS, Jiang H, Stalker TJ, Marchese P, Ruggeri ZM, Brass LF (2005). Eph kinases and ephrins support thrombus growth and stability by regulating integrin outside-in signaling in platelets. Proc Natl Acad Sci USA 102, 9820–9825.
Prévost N, Woulfe DS, Tognolini M, Tanaka T, Jian W, Fortna RR, Jiang H, Brass LF (2004). Signaling by ephrinB1 and Eph kinases in platelets promotes Rap1 activation, platelet adhesion, and aggregation via effector pathways that do not require phosphorylation of ephrinB1. Blood 103, 1348–1355.
Riedl SJ, Pasquale EB (2015). Targeting the Eph system with peptides and peptide conjugates. Curr Drug Targets 16, 1031–1047.
Salvucci O, de la Luz Sierra M, Martina JA, McCormick PJ, Tosato G (2006). EphB2 and ephB4 receptors forward signaling promotes SDF-1-induced endothelial cell chemotaxis and branching remodeling. Blood 108, 2914–2922.
Salvucci O, Tosato G (2012). Essential roles of EphB receptors and Ephrin B ligands in endothelial cell function and angiogenesis. Adv Cancer Res 114, 21–57.
Sawamiphak S, Seidel S, Essmann CL, Wilkinson GA, Pitulescu ME, Acker T, Acker-Palmer A (2010). Ephrin-B2 regulates VEGFR2 function in developmental and tumour angiogenesis. Nature 465, 487–491.
Schnitzer JE, Oh P (1994). Albondin-mediated capillary permeability to albumin. Differential role of receptors in endothelial transcytosis and endocytosis of native and modified albumins. J Biol Chem 269, 6072–6082.
Schubert W, Frank PG, Woodman SE, Hyogo H, Cohen DE, Chow CW, Lisanti MP (2002). Microvascular hyperpermeability in caveolin-1 (–/–) knock-out mice. Treatment with a specific nitric-oxide synthase inhibitor, L-NAME, restores normal microvascular permeability in Cav-1 null mice. J Biol Chem 277, 40091–40098.
Shajahan AN, Timblin BK, Sandoval R, Tiruppathi C, Malik AB, Minshall RD (2004). Role of Src-induced dynamin-2 phosphorylation in caveolae-mediated endocytosis in endothelial cells. J Biol Chem 279, 20392–20400.
Song KS, Sargiacomo M, Galbiati F, Parenti M, Lisanti MP (1997). Targeting of a G alpha subunit (Gi1 alpha) and c-Src tyrosine kinase to caveolae membranes: clarifying the role of N-myristoylation. Cell Mol Biol (Noisy-le-grand) 43, 293–303.
Stan RV, Tse D, Deharvengt SJ, Smits NC, Xu Y, Luciano MR, McGarry CL, Buitendijk M, Nemani KV, Elgueta R, *et al*. (2012). The diaphragms of fenestrated endothelia: gatekeepers of vascular permeability and blood composition. Dev Cell 23, 1203–1218.
Tiruppathi C, Freichel M, Vogel SM, Paria BC, Mehta D, Flockerzi V, Malik AB (2002). Impairment of store-operated Ca^{2+} entry in $TRPC4^{-/-}$ mice interferes with increase in lung microvascular permeability. Circ Res 91, 70–76.
Tiruppathi C, Shimizu J, Miyawaki-Shimizu K, Vogel SM, Bair AM, Minshall RD, Predescu D, Malik AB (2008). Role of NF-κB-dependent caveolin-1 expression in the mechanism of increased endothelial permeability induced by lipopolysaccharide. J Biol Chem 283, 4210–4218.
Tiruppathi C, Soni D, Wang DM, Xue J, Singh V, Thippegowda PB, Cheppudira BP, Mishra RK, Debroy A, Qian Z, *et al*. (2014). The transcription factor DREAM represses the deubiquitinase A20 and mediates inflammation. Nat Immunol 15, 239–247.
Tosato G (2017). Ephrin ligands and Eph receptors contribution to hematopoiesis. Cell Mol Life Sci 74, 3377–3394.
Vassilieva EV, Ivanov AI, Nusrat A. (2009) Flotillin-1 stabilizes caveolin-1 in intestinal epithelial cells. Biochem Biophys Res Commun 379, 460–465.
Vihanto MM, Vindis C, Djonov V, Cerretti DP, Huynh-Do U (2006). Caveolin-1 is required for signaling and membrane targeting of EphB1 receptor tyrosine kinase. J Cell Sci 119, 2299–2309.
Vindis C, Cerretti DP, Daniel TO, Huynh-Do U (2003). EphB1 recruits c-Src and p52Shc to activate MAPK/ERK and promote chemotaxis. J Cell Biol 162, 661–671.
Vogel SM, Gao X, Mehta D, Ye RD, John TA, Andrade-Gordon P, Tiruppathi C, Malik AB (2000). Abrogation of thrombin-induced increase in pulmonary microvascular permeability in PAR-1 knockout mice. Physiol Genomics 4, 137–145.
Wang Y, Nakayama M, Pitulescu ME, Schmidt TS, Bochenek ML, Sakakibara A, Adams S, Davy A, Deutsch U, Lüthi U, *et al*. (2010). Ephrin-B2 controls VEGF-induced angiogenesis and lymphangiogenesis. Nature 465, 483–486.
Williams SE, Mann F, Erskine L, Sakurai T, Wei S, Rossi DJ, Gale, NW, Holt CE, Mason CA, Henkemeyer M (2003). Ephrin-B2 and EphB1 mediate retinal axon divergence at the optic chiasm. Neuron 39, 919–935.
Wu Y, Shroff H (2018). Faster, sharper, and deeper: structured illumination microscopy for biological imaging. Nat Methods 15, 1011–1019.
Wykosky J, Palma E, Gibo DM, Ringler S, Turner CP, Debinski W (2008). Soluble monomeric EphrinA1 is released from tumor cells and is a functional ligand for the EphA2 receptor. Oncogene 27, 7260–7273.
Zimnicka AM, Husain YS, Shajahan AN, Sverdlov M, Chaga O, Chen Z, Toth PT, Klomp J, Karginov AV, Tiruppathi C, *et al*. (2016). Src-dependent phosphorylation of caveolin-1 Tyr-14 promotes swelling and release of caveolae. Mol Biol Cell 27, 2090–2106.